Angewandte International Edition Chemie

Molecular Engineering

How to cite: *Angew. Chem. Int. Ed.* **2020**, *59*, 10160–10172
International Edition: doi.org/10.1002/anie.201916357
German Edition: doi.org/10.1002/ange.201916357

Quantitative Design of Bright Fluorophores and AIEgens by the Accurate Prediction of Twisted Intramolecular Charge Transfer (TICT)

Chao Wang+, Qinglong Qiao+, Weijie Chi, Jie Chen, Wenjuan Liu, Davin Tan, Scott McKechnie, Da Lyu, Xiao-Fang Jiang, Wei Zhou, Ning Xu, Qisheng Zhang, Zhaochao Xu, and Xiaogang Liu**

Abstract: *Inhibition of TICT can significantly increase the brightness of fluorescent materials. Accurate prediction of TICT is thus critical for the quantitative design of high-performance fluorophores and AIEgens. TICT of 14 types of popular organic fluorophores were modeled with time-dependent density functional theory (TD-DFT). A reliable and generalizable computational approach for modeling TICT formations was established. To demonstrate the prediction power of our approach, we quantitatively designed a boron dipyrromethene (BODIPY)-based AIEgen which exhibits (almost) barrierless TICT rotations in monomers. Subsequent experiments validated our molecular design and showed that the aggregation of this compound turns on bright emissions with ca. 27-fold fluorescence enhancement, as TICT formation is inhibited in molecular aggregates.*

Introduction

The chemistry of fluorescent dyes and probes is currently experiencing a rapid evolution from trial-and-error to molecular engineering.[1] During this evolution, computational chemistry is playing an exceedingly important role by elucidating fluorescence switching mechanisms and affording improved molecular designs at minimal cost compared to the experimental screening of fluorophores.[2] The wide acceptance of computational chemistry by dye chemists, however, critically depends on its reliability in rationalizing and predicting experimental results.

Among various computational methods, time-dependent density functional theory (TD-DFT) is rapidly becoming the default choice in studying photophysics and photochemistry.[3] The excited-state properties of many fluorescent molecules are key in dye chemistry and are often challenging to experimentally measure, yet TD-DFT affords these properties with a good balance of computational cost and accuracy.[4] Indeed, the past two decades have witnessed the undeniable success of TD-DFT in the design and creation of new and improved fluorophores.[5] However, despite its impact, many dye chemists are still skeptical and critical about the reliability of TD-DFT, especially because the misuse of TD-DFT predictions leads to significantly different outcomes even for experimentally verified photophysical processes.[6] Obtaining a reliable mechanistic understanding towards quantitative molecular design, however, requires a comprehensive consideration of many factors, such as the diversity of fluorophore structures, their embedded environment, and the choice of computational recipes. Unfortunately, owing to the formidable workload, such sought-after benchmarking studies are often missing.

To this end, one classical and representative problem is the reliable prediction of twisted intramolecular charge transfer (TICT).[7] The TICT model was first proposed by Grabowski and co-workers, for interpreting the unusual dual fluorescence bands of 4-(dimethylamino)benzonitrile (DMABN).[8] In the TICT state, the electron-donating moiety (D) and/or the electron-accepting moiety (A) of a quasi-planar fluorophore rotates towards a nearly perpendicular alignment upon photoexcitation. During this rotation, the degree of intramolecular charge transfer (ICT) greatly intensifies. This leads to the formation of a charge-separated species that is highly reactive and non-emissive. It was also shown that the TICT model could explain the fluorescence characteristics of many other organic fluorophores.[9]

---

[*] Dr. C. Wang,[+] Dr. W. Chi, Dr. D. Tan, Prof. Dr. X. Liu
Fluorescence Research Group, Singapore University of Technology and Design
8 Somapah Road, Singapore 487372 (Singapore)
E-mail: xiaogang_liu@sutd.edu.sg

Dr. C. Wang,[+] Dr. Q. Qiao,[+] J. Chen, W. Liu, W. Zhou, N. Xu, Prof. Dr. Z. Xu
CAS Key Laboratory of Separation Science for Analytical Chemistry, Dalian Institute of Chemical Physics, Chinese Academy of Sciences
457 Zhongshan Road, Dalian 116023 (China)
E-mail: zcxu@dicp.ac.cn

Dr. S. McKechnie
Department of Physics, Kings College London
London WC2R 2LS (UK)

D. Lyu
Department of Chemistry, National University of Singapore
21 Lower Kent Ridge Rd, Singapore 119077 (Singapore)

Dr. X. Jiang
School of Physics and Telecommunication Engineering
South China Normal University, Guangzhou 510006 (China)

Prof. Dr. Q. Zhang
MOE Key Laboratory of Macromolecular Synthesis and Functionalization, Department of Polymer Science and Engineering
Zhejiang University, Hangzhou 310027 (China)

[+] These authors contributed equally to this work.

Supporting information and the ORCID identification number(s) for the author(s) of this article can be found under: https://doi.org/10.1002/anie.201916357.

Modulating TICT formation in fluorophores has led to the creation of numerous functional materials, such as bright and photostable fluorophores,[9g,10] polarity probes,[11] viscosity sensors,[12] photosensitizers,[13] dark quenchers,[14] and luminogens with aggregation-induced emission characteristics (AIEgens).[15] The quantitative design of such fluorophores requires a deep mechanistic understanding. Yet, the existence of TICT in many fluorophores remains controversial, and the detailed understanding of related processes at the molecular level is still incomplete. For instance, Lavis et al. suggested that inhibiting TICT is a plausible mechanism to explain the improved brightness and photostability of azetidine-substituted fluorophores.[10a] In contrast, these improvements were attributed to reduced hydrogen bond quenching in coumarins.[16] Notably, Tang group reported that AIE can be triggered through the suppression of TICT in the molecular aggregates of boron dipyrromethene (BODIPY) derivatives.[15] However, it remains challenging to precisely identify the chemical bond involved in TICT rotations, especially when multiple potential rotors are available in a molecule. These mechanistic disagreement and challenges demand accurate theoretical calculations to reconcile experimental results, as theoretical calculations are likely the only tool available for chemists to directly visualize the short-lived TICT states.[17] However, establishing an accurate and generalizable computational approach for predicting TICT formations in different systems seems an inaccessible goal, because the appropriate use of TD-DFT calculations, to the best of our knowledge, remains controversial.

In an important study, the ubiquitously used B3LYP functional-based results suggested that the emission of 6-propionyl-2-(dimethylamino)naphthalene (PRODAN), a classical polarity probe, stems from the TICT state.[18] However, subsequent experimental work by Abelt and co-workers provided unambiguous evidence that the emission of PRODAN is from a planar conformation.[19] The inability of the B3LYP functional to handle charge transfer states and related Coulomb interactions (that is, in the TICT state) prompted the development of many modern range-separated functionals (such as CAM-B3LYP and ωB97XD).[20] Meanwhile, the charge transfer problem has also been addressed by other newly developed global hybrid functionals (such as M062X).[21] One major difference between these functionals is the amount of hybridization with Hartree–Fock (HF) exchange, which compensates the underestimation of excitation energies of pure functionals in the charge-transfer states.[22] Several empirical and non-empirical tuning methods have also been introduced to quantify the optimal amount of HF exchange for various charge transfer systems.[23]

With the availability of these functionals and methods, many important works have been performed to model TICT using TD-DFT and provided valuable insights.[24] It is shown that range-separated functionals (such as CAM-B3LYP) offer a good description of the overall potential energy surface (PES) during the TICT formation in vacuo.[25] However, numerous experimental works have shown that appreciable TICT formation occurs only in polar solvents, as polar solvents greatly stabilize the charge-separated TICT species.[9a,b,e,26] Unfortunately, acceptable TD-DFT results obtained in vacuo (owing to error cancellation) are no longer applicable when solvent effects are included in calculations. Pedone showed that the CAM-B3LYP combined with the state-specific (SS) solvation formalism provides a qualitatively correct description to the TICT formation of Coumarin 152 (C152) in various solvents, provided that the molecular structures are optimized using B3LYP (which failed in vacuo) coupled with the linear-response (LR) solvation formalism. However, Mennucci and co-workers pointed out that this mixed remedy exaggerated the tendency of TICT formation.[27]

Herein, we formulated a TD-DFT computational recipe for accurately modeling TICT formation. We validated the reliability of this recipe in 14 types of popular fluorophores, in close agreement with experimental data in various solvent mediums. This approach enabled us to revisit the TICT mechanism of PRODAN in polar solvents and quantitatively design PRODAN derivatives with enhanced one-photon and two-photon bioimaging performance via inhibiting TICT. The prediction power of our approach also allowed us to quantitatively design a new TICT-based AIEgen. While our results mainly concern TICT formations, we expect that our approach is also applicable to other fluorophores involving multiple excited states with different degrees of charge transfer (that is, photoinduced electron transfer).

Results and Discussion

The TICT Model of Organic Fluorophores

Upon photoexcitation, a fluorophore could experience a transition from the initially populated locally excited (LE) or intramolecular charge-transfer (ICT) state to the TICT state (Figure 1 a). The LE/ICT state corresponds to a quasi-planar molecular conformation and is usually highly fluorescent with a large radiative decay rate. In contrast, the circa 90° twisted TICT state is typically non-emissive. The transition rates between the LE/ICT and TICT states, k_a and k_b, can be derived from the activation energies, E_a and $E_b = \Delta H + E_a$, using the Arrhenius equation and assuming an elementary reaction, respectively (Figure 1 b). These transition rates determine the nonradiative decay rate from the TICT state, which in turn control the fluorescence quantum yield of the fluorophore. The larger the transition rate is, the larger the nonradiative decay rate will be. Accordingly, E_a and $-\Delta H$ play a significant role in modulating the fluorescence output.

Theoretically, the LE/ICT to TICT transition can be modeled by calculating the S_1 PES along the rotation angle (θ) of the donor (or the acceptor) fragment (Figure 1 c–f). The rotation barrier (E_{RB}) and driving energy (E_{DE}), corresponding to E_a and $-\Delta H$, respectively, are crucial to evaluate the possibility of populating the TICT state. A positive E_{DE} indicates that the TICT. formation cannot spontaneously occur (Figure 1 c,d). When $E_{RB} > 0$ and $E_{DE} < 0$, both LE/ICT and TICT states become populated (Figure 1 e). The smaller E_{RB} and the more negative E_{DE} are, the more likely TICT transitions will take place. When E_{RB} approaches 0, the TICT

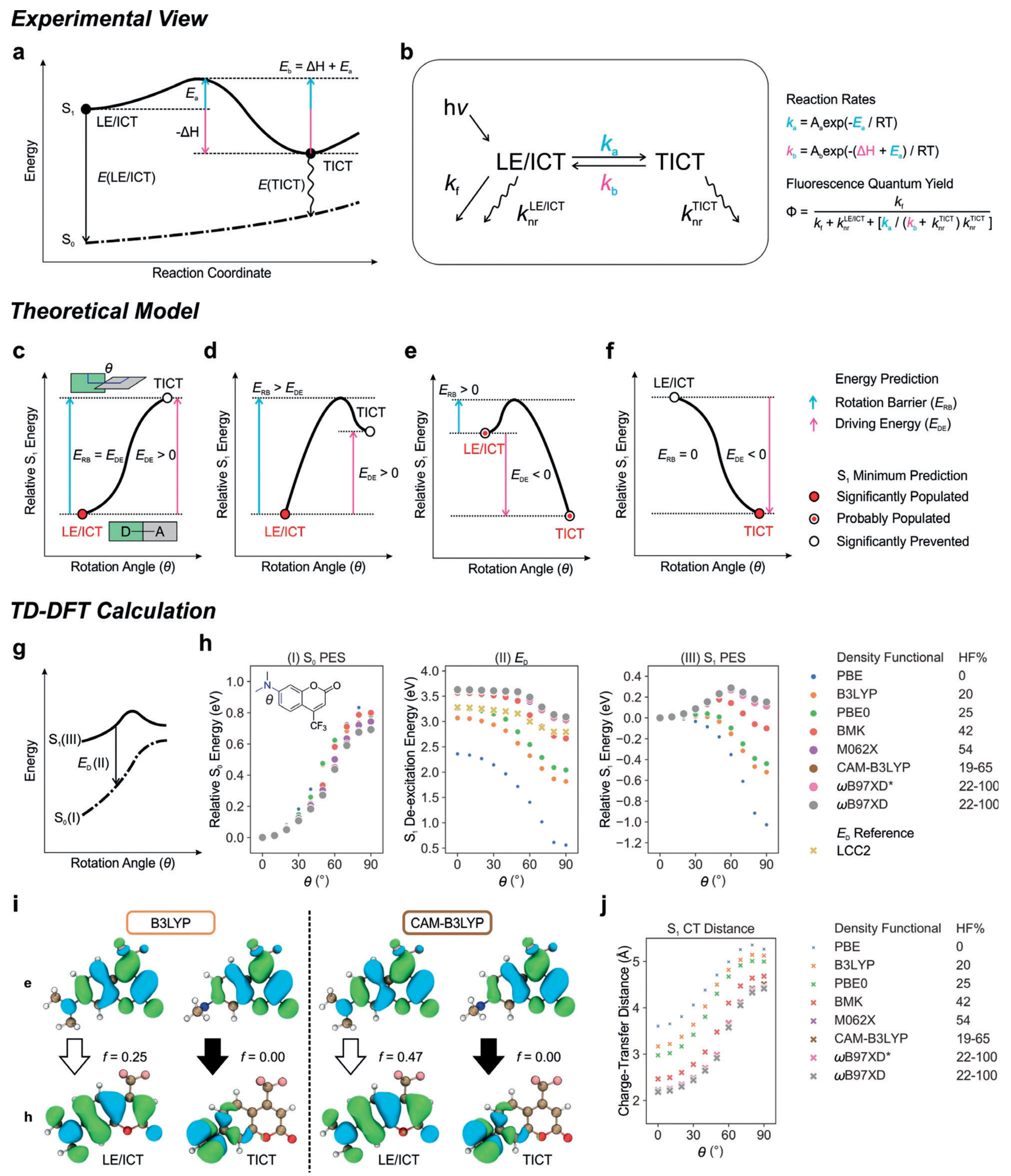

Figure 1. a),b) Experimental view of a) the LE/ICT→TICT photoreaction and b) corresponding calculations of reaction rates (k_a and k_b) and fluorescence quantum yield (Φ) using Arrhenius equation (assuming elementary reactions). Here k_f and k_{nr} denote the radiative and nonradiative rate, respectively. c),f) The theoretical model of describing the LE/ICT→TICT photoreaction by plotting S_1 PES along the rotation angle (θ) towards the formation of c),d) LE/ICT excited states; e) both LE/ICT and TICT excited states f) TICT excited state. g),h) TD-DFT calculations of g) de-excitation energy (E_D), S_1 and S_0 PESs, and h) a case study of C152 using different functionals in comparison with the LCC2 reference in vacuo. i) The distribution of hole (h) and electron (e) natural transition orbitals (NTOs) of LE/ICT and TICT states calculated at the B3LYP and CAM-B3LYP levels of theory in vacuo. The oscillator strength (f) is labeled in the inset. j) Charge transfer distance as a function of rotation angle (θ) calculated using different functionals.

state will readily form, causing substantial fluorescence quenching (Figure 1 f).

Modeling TICT Formation of C152 In Vacuo

TD-DFT can be used to calculate the corresponding relative S_1 PES (with $E(S_1, \theta=0)$ as the reference), which can be decomposed into the relative S_0 PES and S_1 de-excitation energy (Figure 1g). The results of TD-DFT calculations strongly depend on the fraction of HF exchange (HF%) in different functionals (Supporting Information, Sections 1.2 and 1.3, Figure S1).

To fully evaluate the performance of different functionals in modeling TICT formations, we calculated the S_0 PESs, the S_1 de-excitation energies (vertical emissions) and resulting S_1 PESs in vacuo, as a function of the dimethylamino group rotation (Figure 1h), based on the optimized S_1 molecular structures of C152. During these calculations, we employed eight representative functionals (including one pure functional, four global hybrid functionals, and three range-separated functionals) with different HF%. We also performed high-level LCC2 calculations on C152 as a benchmark. LCC2 has been shown to be a reliable approach to including electron-correlation effects and modeling charge transfer excitations.[28] It is noteworthy to mention that previous experimental studies have demonstrated that C152 could enter the TICT state, but only in polar solvents. For example, the quantum yield (Φ) of C152 is as high as 0.97 in cyclohexane (a non-polar solvent),[29] but drops to 0.28 in acetonitrile (a polar solvent).[30]

Our results show that all functionals provide similar S_0 PES profiles (Figure 1h (I)). While the relative S_0 energy differences between functionals slightly rise with the increase in θ, these differences are in general small (<0.11 eV).

In stark contrast, the differences in the S_1 de-excitation energies are substantial among various functionals (up to 2.53 eV; Figure 1h (II)). In comparison to LCC2 results, pure functional PBE constantly underestimates the de-excitation energy by >0.92 eV. The underestimation tends to become more severe (up to 2.24 eV) as θ increases. For global hybrid functionals with low HF%, such as B3LYP and PBE0, the calculated de-excitation energy in the LE/ICT state ($\theta=0°$) is very close to that of LCC2, suggesting that they are good choices for modeling fluorophores with a weak/moderate degree of ICT. However, these functionals produce substantial errors (up to 0.98 eV) after $\theta=50°$, owing to the underestimation of de-excitation energy when charge transfer intensifies in C152 (Figure 1h–j). The S_1 de-excitation energies calculated by global hybrid functionals with high HF% and range-separated functionals, such as M062X, CAM-B3LYP, and ωB97XD, are consistently larger than LCC2 results by about 0.35 eV. Nevertheless, results from these functionals fit the general profile of LCC2 references. We also tested the ionic potential (IP) tuning scheme, which shows little improvement (Supporting Information, Section 1.4).

Owing to the considerable differences in the S_1 de-excitation energy, all tested functionals generated noticeably different S_1 PESs (Figure 1h (III)). It should be emphasized that for modeling TICT formation, it is critical to reproduce the S_1 PES profile, rather than the absolute values of de-excitation energies. As a consequence, range-separated functionals and M062X correctly predicted that the TICT state of C152 is not stable in vacuo, which is in good agreement with experimental data.[9e] In contrast, pure and global hybrid functionals with low HF% suggest substantial TICT formations even in vacuo and can be deemed as computational artifacts.

Overall, our data show that both range-separated functionals and global hybrid functional with large HF% (such as M062X) are reliable in modeling TICT formation in vacuo.

Modeling TICT Formation of C152 in Solvents

Next, we benchmarked different functionals in various solvents of different polarities (including cyclohexane, ethanol, water, and water with explicit solvent molecules to mimic hydrogen-bond interactions) using the SMD model to simulate the solvent effects. We considered three solvation formalisms: 1) linear response (LR); 2) corrected linear response (cLR); and 3) state-specific (SS). The latter two formalisms are (in principle) more accurate, for accounting for polarization changes of the solvent in response to the electronic density rearrangements of the fluorophore.

Our results using the LR formalism showed that the overall S_1 PES profiles in solvents are similar to those in vacuo (Figure 2a). For example, the pure functional PBE underestimates the de-excitation energies in charge transfer states (Supporting Information, Figure S2a) and suggests almost barrierless transitions to the TICT state in all solvents. In contrast, global hybrid functionals with large HF% and range-separated functionals indicate that the TICT state is energetically unstable in comparison to the LE/ICT state (with large E_{RB} and positive E_{DE}) in various solvents. These computational results, however, are inconsistent with the experimental results, which showed considerable TICT formations of C152 only in polar solvents. Any functionals combined with LR combinations failed to predict the increasing TICT formation with the growing solvent polarity. As such, we do not recommend the use of LR solvation formalism for constructing S_1 PES and describing the TICT formation process.

Subsequently, we calculated the S_1 PES using various functionals in combination with the cLR solvent formalism (Figure 2b). With cLR, all functionals correctly predicted that the TICT state becomes increasingly stable (with the increasing magnitude of E_{DE}) when the solvent changes from cyclohexane to water (Figure 2e). However, the rotation barrier (E_{RB}) to the more stable TICT state is almost negligible for PBE, B3LYP, and PBE0 in all solvents (Figure 2d), which is inconsistent with the bright emission of C152 in cyclohexane. In contrast, global hybrid functionals with significant HF% (such as M062X) and range-separated functionals (such as CAM-B3LYP and ωB97XD) yielded reasonable energy barriers.

Finally, we tested the SS solvent formalism for constructing the S_1 PESs (Figure 2c). In comparison to cLR data, we noted that the SS formalism leads to a significant increase in

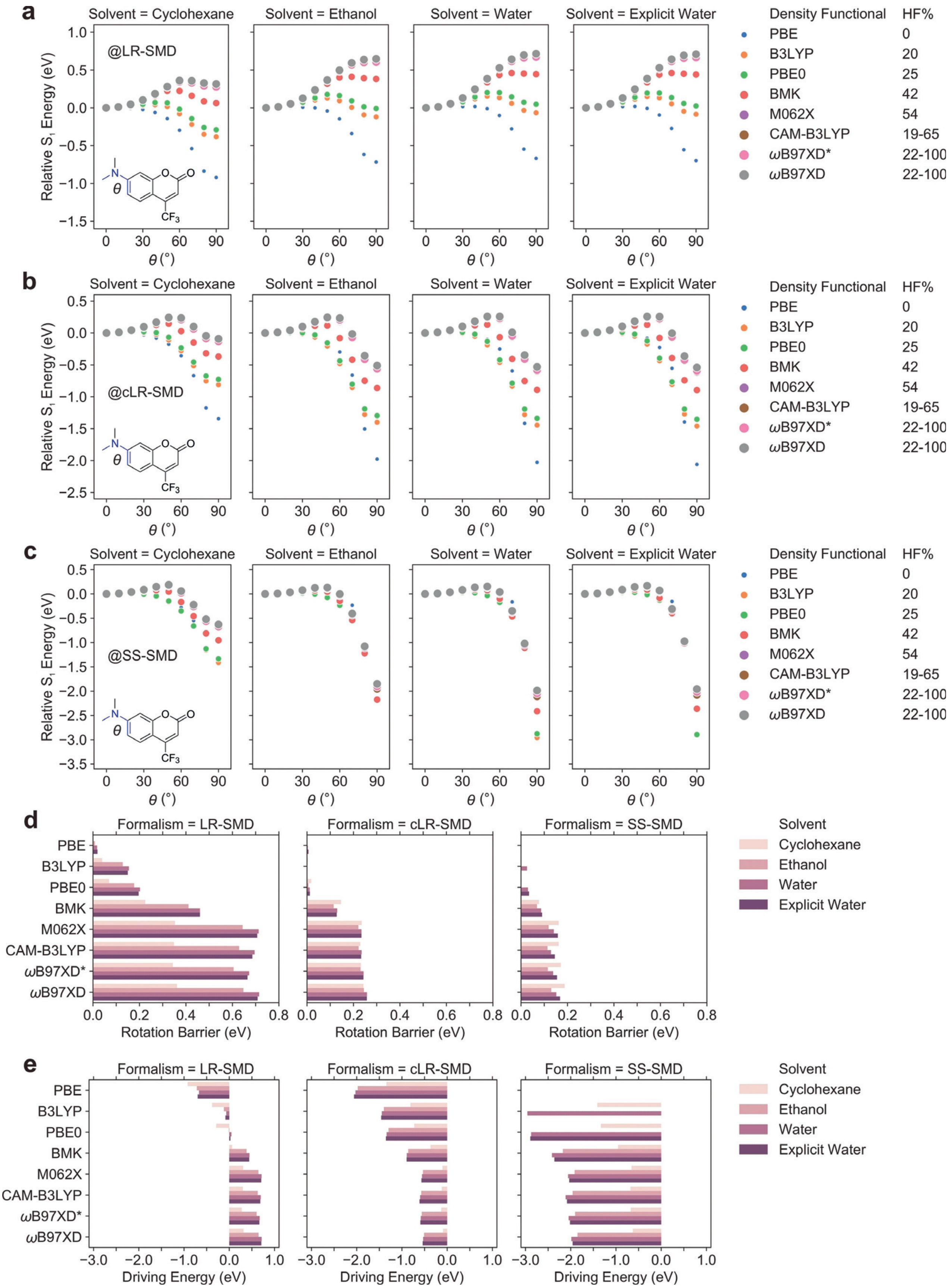

Figure 2. Relative S$_1$ PES of C152 as a functional of θ using a) LR-SMD, b) cLR-SMD, and c) SS-SMD solvent formalisms in cyclohexane, ethanol, water, and explicit water solutions and the associated d) rotation barriers and e) driving energies for TICT formations.

the magnitude of the driving energy along with a slight reduction in E_{RB} for the TICT formation (Figure 2 d,e). This is because the SS formalism significantly underestimates the de-excitation energies in the TICT states (Supporting Information, Figure S2c). As a result, it overestimates the population of the TICT states even in cyclohexane, conflicting with experimental observations ($\Phi = 0.97$ in cyclohexane).[29] Other groups have also noted the underestimation of TICT de-excitation energy by the SS solvent formalism.[27]

The impact of basis sets, solvent models, and solvation free energy is also compared and the differences on describing S_1 PES are negligible (Supporting Information, Figure S3).

Based on these results, we concluded that the combination of CAM-B3LYP (and other functionals including M062X, ωB97XD, and ωB97XD*) with cLR solvent formalism is reasonable in reproducing the S_1 PES for predicting TICT formations in various solvents. In subsequent calculations, we will focus on the CAM-B3LYP/SMD-cLR level of theory.

Modeling TICT of Various Fluorophores in Solvents

Next, we evaluated its applicability in other organic fluorophores. To this end, the Lavis group has shown that the azetidinyl substitution of di-alkylated amino groups greatly improves the quantum yields of a wide range of organic fluorophores.[10a] They also suggested that these improvements are probably related to the inhibition of TICT. Alternative explanations (that is, hydrogen-bond interactions) have been suggested for these quantum yield improvements.[16]

We decided to resolve this conflict by modeling the TICT formation in these fluorophores, including coumarin, nitrobenzoxadiazole (NBD), 5-(dimethylamino)naphthalene-1-sulfonyl (Dansyl), O/C/Si-rhodamines, rhodol, acridine, oxazine, naphthalimide, and phthalimide derivatives (Figure 3 a). Our results revealed larger rotation barriers and smaller magnitude of driving energies for TICT formations in azetidinyl substituted compounds than in the dialkylated analogues (Figure 3 b, Supporting Information, Figures S4, S5). The TICT model thus well explained the quantum yield enhancement in azetidinyl substituted fluorophores. It also suggests that our approach applies to the fluorophores of various degrees of charge transfer (Supporting Information, Figures S6–S19).

Besides, we also investigated 4-(dimethylamino)benzonitrile (DMABN) and 4-(azetidinyl)benzonitrile (P4C) in diethyl ether (Supporting Information, Figure S20; Section 2.4). DMABN is one of the few examples where the TICT state is weakly emissive at about 420 nm in diethyl ether.[31] With the azetidinyl substitution, the TICT emission band of P4C disappeared.[32] The different emission spectra of DMABN and P4C provided compelling experimental evidence on the role of the azetidinyl group in suppressing TICT. Interestingly, our calculations also showed that P4C is more resistant to TICT than DMABN owing to a higher rotation barrier and smaller magnitude of driving energy (−0.8 eV for P4C vs. −0.92 eV for DMABN), which is in good agreement with the reported data (Supporting Information, Figure S20d).

Overall, our calculations demonstrated that the azetidinyl substitution played an important role in weakening the tendency of populating TICT states. Moreover, the CAM-B3LYP/cLR-SMD level of theory provides a good description of the TICT formation process in a broad range of organic fluorophores and various solvents. The plot of S_1 PESs and the corresponding comparison of rotation barriers and driving energies between fluorophores can serve as a reliable approach for predicting the tendency of TICT formations. However, we did not consider, and thus could not rule out other possible fluorescence quenching mechanisms (that is, hydrogen-bond interactions).

Quantitative Design of PRODAN Derivatives with Bright Emissions

Inspired by the successful modeling of TICT formations in these fluorophores, we continued to resolve a two-decade-long debate on the fluorescence mechanism of PRODAN.[33] PRODAN and their derivatives received significant research attention, owing to their excellent biocompatibility and polarity sensitivity.[10b,34] Previous studies have proposed the existence of LE/ICT and TICT excited states in PRODAN.[35] However, the TICT state was considered as an inconsequential artifact by some researchers.[36] By investigating PRODAN derivatives whose dimethylamino or propionyl functional groups have been fixed in co-planar orientation using alkylation (Figure 4 a), several experimental studies have confirmed that the fluorescence of PRODAN originates from the LE/ICT state[19a,b] or LE states with charge transfer character[37] (the planar conformation). However, it is noted that PRODAN displayed sub-optimal quantum yields in polar solvents like water.[37] Such moderate quantum yields have been attributed to hydrogen-bonding induced quenching,[19c,38] yet the mechanistic origin of the suboptimal brightness of PRODAN remains unclear.

To illuminate the photophysical mechanism of PRODAN and design improved dipolar fluorophores, we applied our computational approach to investigate the excited-state properties of PRODAN. Unless otherwise specified, isomer B configuration is used for PRODAN throughout the study due to its lower total energy than isomer A (Supporting Information, Figure S21). The calculated S_1 PES suggests that the N-TICT state (ca. 90° rotations around the dimethylamino group) is energetically favorable in water (Figure 4 b), while the O-TICT state (ca. 90° rotations around the propionyl group) is not stable in all solvents (Figure 4 c). The comparison of S_1 PES between implicit and explicit water revealed that hydrogen bonding has little influence on the TICT formation. Different exchange-correlation functionals were also benchmarked, supporting the formation of the N-TICT state and the prevention of the O-TICT state, and corroborating the validity of our TICT computational approach (Supporting Information, Figures S22–S25).

To prevent the population of N-TICT states and improve the fluorescence quantum yield of PRODAN in water, we

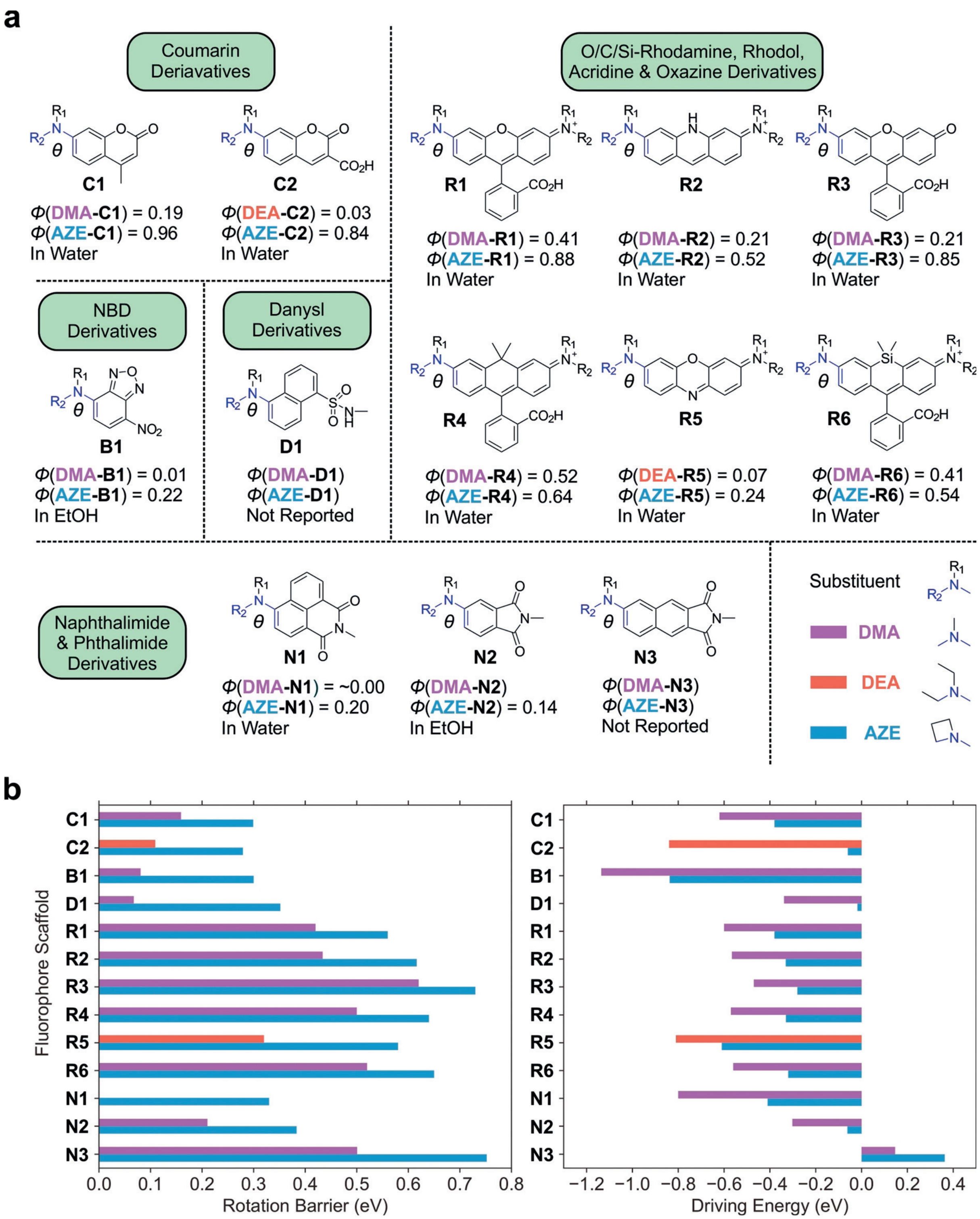

Figure 3. a) The comparison of fluorescence quantum yields (Φ) between dimethylamino (DMA), diethylamino (DEA), and azetindyl (AZE) substituted coumarin (C1–C2), NBD (B1), Dansyl (D1), O/C/Si-rhodamine, rhodol, acridine, and oxazine (R1–R6), naphthalimide, and phthalimide (N1–N3) fluorophores. b) The corresponding rotation barriers (E_{RB}) and driving energies (E_{DE}) for TICT formations calculated at the CAM-B3LYP/cLR-SMD level in water. Fluorescence quantum yields of O/C/Si-rhodamine, rhodol, acridine, oxazine, and coumarin derivatives are adapted from Ref. [10a]. Fluorescence quantum yields of NBD dyes are adapted from Ref. [39]. Fluorescence quantum yields of naphthalimide and phthalimide dyes are adapted from Ref. [9g].

designed 2-acetyl-6-(dimethylamino)naphthalene (ACEDAN)-like fluorophores applying azetidinyl (P4), pyrrolidinyl (P5) and piperidinyl (P6) substitutions to replace the dimethylamino (P2) moiety (Figure 4a). Our TD-DFT calculations predict that the rotation barriers and driving energies of P4 ($E_{RB} = 0.38$ and $E_{DE} = -0.14$ eV) and P5

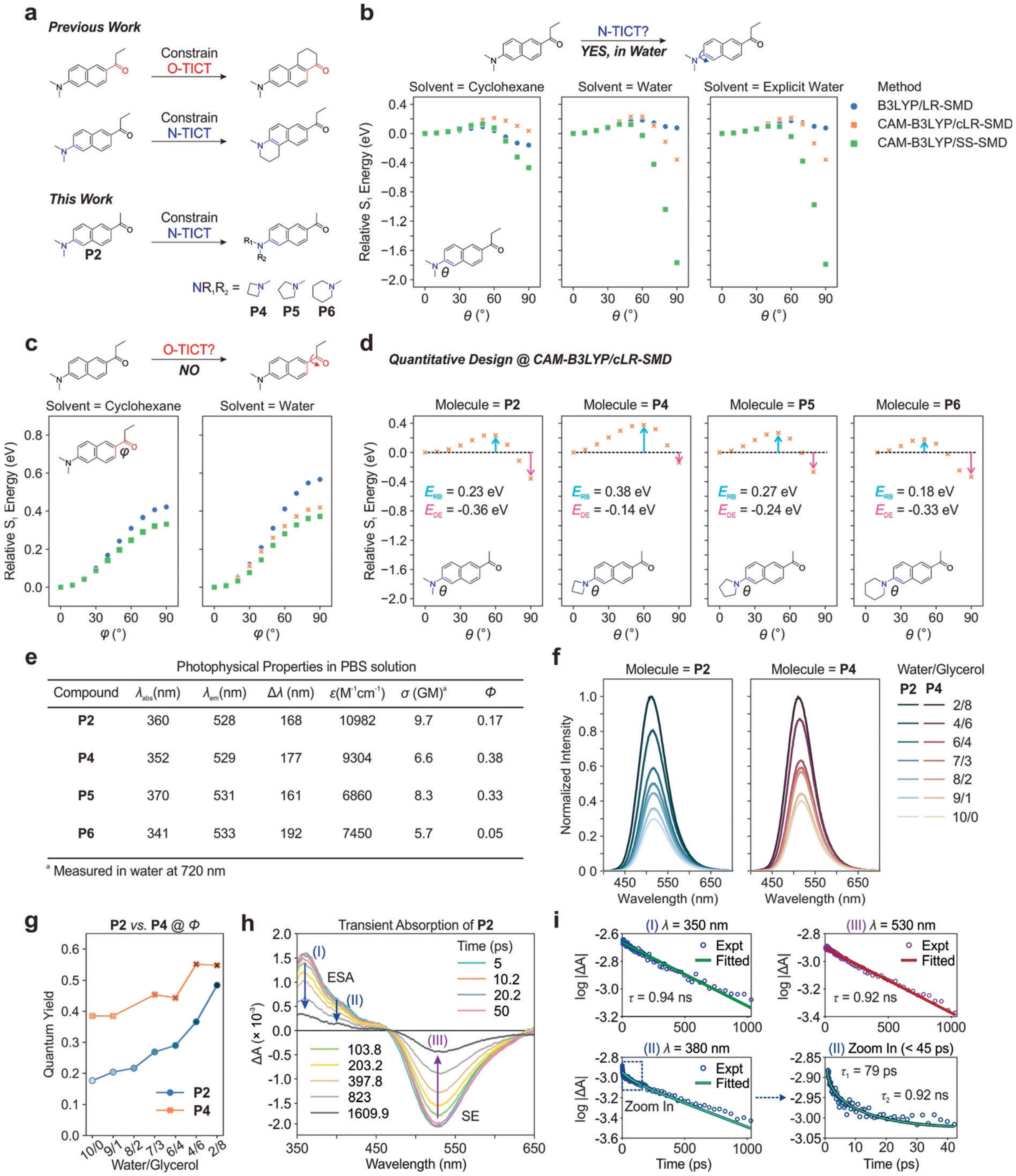

Photophysical Properties in PBS solution

Compound	λ_{abs}(nm)	λ_{em}(nm)	$\Delta\lambda$ (nm)	ε($M^{-1}cm^{-1}$)	σ (GM)[a]	Φ
P2	360	528	168	10982	9.7	0.17
P4	352	529	177	9304	6.6	0.38
P5	370	531	161	6860	8.3	0.33
P6	341	533	192	7450	5.7	0.05

[a] Measured in water at 720 nm

Figure 4. a) A general comparison of PRODAN derivatives in previous work (N-alkylation) and this work (azetidinyl, pyrrolidinyl, and piperidinyl substitution). b),c) Calculated relative S_1 energy as a function of the b) N-TICT (θ) and c) O-TICT (φ) rotation angle using various methods in cyclohexane, water, and explicit water. d) Relative S_1 energy as a function of the N-TICT rotation angle (θ) for P2, P4, P5, and P6 calculated at the CAM-B3LYP/cLR-SMD level in water solution. e) Absorption (λ_{abs}) and emission maxima (λ_{em}), Stokes shifts ($\Delta\lambda$), molar extinction coefficients (ε) and quantum yields (Φ) of P2, P4, P5, and P6 measured in PBS solution. f) The relative fluorescence intensities of P2 and P4 as a function of water/glycerol volume fractions and g) the corresponding quantum yields. h) Transient absorption spectra of P2 in PBS solution and i) the relevant decay dynamics of ESA band I (350 nm), ESA band II (380 nm), and EM band III (530 nm).

($E_{RB} = 0.27$ and $E_{DE} = -0.24$ eV) are larger than that of P2 ($E_{RB} = 0.23$ and $E_{DE} = -0.36$ eV), indicating the N-TICT states will be less likely to form in P4 and P5 than in P2 (Figure 4d). In contrast, the TICT states should populate more easily in P6 than in P2 as the rotation barrier of P6 ($E_{RB} = 0.18$ eV) is smaller. We thus expect that P4 and P5 should possess much higher quantum yields than P2 does, because of their stronger TICT resistance.

Validation of Molecular Design Strategies

To validate our computational predictions, we synthesized the compounds mentioned above (Supporting Information, Figures S27–S39, Schemes S1–S6) and measured their absorption and emission spectra in different solvents (Supporting Information, Figure S40, Table S2). In PBS solution (Figure 4e), the first absorption bands of these compounds peaked around 341–370 nm, and the emission maxima were at about 530 nm. As expected, the quantum yields of P4 ($\Phi = 0.38$) and P5 ($\Phi = 0.33$) are about twice than that of P2 ($\Phi = 0.17$), while the quantum yield of P6 ($\Phi = 0.05$) is significantly lower. These results are in excellent agreement with our theoretical predictions.

Moreover, the molar extinction coefficients of P2 ($\varepsilon = 10982\,\mathrm{M}^{-1}\mathrm{cm}^{-1}$) and P4 ($\varepsilon = 9304\,\mathrm{M}^{-1}\mathrm{cm}^{-1}$) are higher than those of P5 ($\varepsilon = 6860\,\mathrm{M}^{-1}\mathrm{cm}^{-1}$) and P6 ($\varepsilon = 7450\,\mathrm{M}^{-1}\mathrm{cm}^{-1}$; Figure 4e). The overall brightness of P4 thus demonstrates a nearly one-fold increase compared to that of P2. We also noted that the two-photon cross-sections (σ) of these compounds are comparable at 720 nm considering the measurement uncertainty (about 10%). Again, this is in good agreement with theoretical calculations (Supporting Information, Figure S26).

Clarifications of TICT and Hydrogen-Bond Interactions

To elucidate the relationship between fluorescence enhancement and TICT formation, we measured the fluorescence intensities (Figure 4f) and quantum yields (Figure 4g) of P2 and P4 in water–glycerol mixtures of varying volume ratios. It was observed that the relative fluorescence intensity of P2 and P4 gradually increases when the water/glycerol ratio changed from 10/0 to 2/8. The proton donating abilities of water and glycerol are very similar (hydrogen bond donating strength $\alpha = 1.17$ and 1.21 for water and glycerol, respectively),[40] which suggests that varying water/glycerol fractions barely influences the hydrogen-bonding interactions of solvents with P2 and P4. Therefore, the enhancement of fluorescence intensities of P2 and P4 can be attributed to TICT inhibition as glycerol is significantly more viscous and less polar than water is.

Notably, the increase of quantum yields is more significant in P2 than in P4; P2 and P4 exhibit comparable quantum yield ($\Phi = 0.48$ vs. 0.55) when the volume fraction of glycerol rises to 80%. These results suggest that P2 is more vulnerable to the TICT formation. While P4 is also prone to the TICT formation, it exhibited much stronger TICT resistance. These results are fully consistent with our TD-DFT calculations.

Nevertheless, their suboptimal and comparable quantum yields in the water–glycerol mixture (volume fractions = 2/8) also validates the presence of hydrogen bond quenching (HBQ) phenomenon in PRODAN, as pointed out in previous studies.[19b,c,38] Indeed, as we changed the solvent to DMSO for avoiding hydrogen bond interactions around the oxygen atoms, the quantum yields of both P2 and P4 increased substantially (Supporting Information, Table S2).

Transient Absorption Studies

To further explore the excited state dynamics and validate the TICT formations, we measured the transient absorption spectra of P2 and P4 (Figure 4h,i). Two excited-state absorption bands (ESA, I, and II) and one stimulated emission band (SE, III) were observed in P2. We assigned the ESA band (I) to the emissive ICT state as its lifetime ($\tau = 0.94$ ns) is comparable to that of the SE band (III) ($\tau = 0.92$ ns). The ESA band (II) is composed of two different excited states with a double exponential decay ($\tau_1 = 79$ ps and $\tau_2 = 0.92$ ns, respectively); the latter is consistent with that of the ICT state. We thus attributed the short lifetime ($\tau_1 = 79$ ps) to the TICT state, as it is comparable to that of a fully charge-separated excited state in our previous study.[2b]

A similar transient absorption profile is also observed in P4 (Supporting Information, Figure S41a,b). The ESA band (II) at 391 nm consists of a double exponential decay profile, suggesting the co-existence of the non-emissive TICT ($\tau_1 = 79$ ps) and emissive ICT ($\tau_2 = 1.37$ ns) states.

By combing the experimental and theoretical results, we concluded that PRODAN and ACEDAN could form non-emissive TICT states in water, resulting in their suboptimal quantum yields; hydrogen-bonding interactions also partially contribute to their fluorescence quenching. We have also demonstrated that the azetidinyl group is capable of (partially) suppressing TICT formation, thus endowing P4 with an approximately one-fold increase in quantum yield and brightness in water.

Bioimaging Applications Using P4

To demonstrate the utilities of our newly designed fluorophore, we deployed both P2 and P4 in one-photon (OP) and two-photon (TP) imaging of live HeLa cells (Figure 5a). Our results showed that both P2 and P4 showed excellent permeability to cell membranes. Moreover, P4 afforded brighter images than P2 did; the maximum fluorescence intensity of P4 doubled that of P2 (Figure 5b). The statistical distribution of intensity in these images also suggest that P4 outperforms P2 in OP and TP imaging applications (Supporting Information, Figure S42). The higher brightness of P4 is mainly attributed to its higher quantum yield than that of P2, as a result of enhanced TICT resistance.

We also studied the stability of P2 and P4 in fixed HeLa cells (Figure 5c). The relative intensity of P4 decreases within the first 5 frames and then plateaus at around 0.82. In comparison to P4, the intensity of P2 continuously decays as a result of considerable TICT formation, which deteriorates its photostability. Similar behaviors of P2 and P4 were also observed in live HeLa cells (Supporting Information, Figure S43).

These imaging experiments revealed that P4 is more recalcitrant towards the TICT formation than P2 and exhibited higher fluorescence brightness and photostability, which facilitates the imaging utilities in both fixed and live HeLa cells.

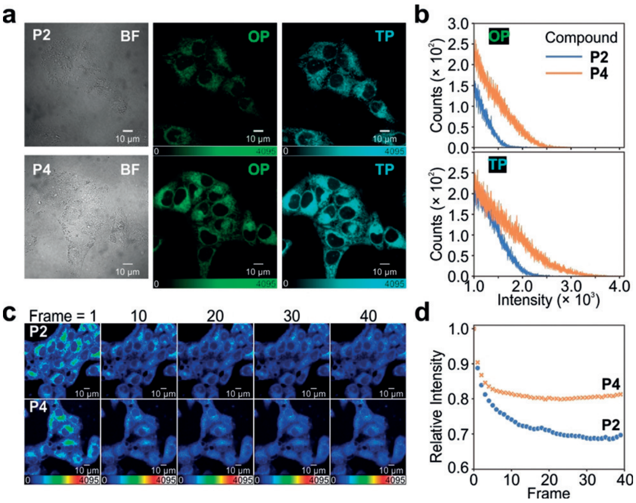

Figure 5. a) Bright-field (BF), one-photon (OP), and two-photon (TP) bioimaging of P2 and P4 in live HeLa cell and b) the corresponding photon statistics. c) The OP imaging of P2 and P4 at different frames (14.4 seconds/frame) in fixed HeLa cells and d) the corresponding relative fluorescence intensity decays.

Quantitative Development of a TICT-based AIEgen

AIEgens have attracted considerable interest in a wide range of applications, that is, the organic light-emitting diodes,[41] photodynamic therapy agents,[42] and biosensors.[43] Formulating rational design protocols is critical to accelerate the development of AIEgens and expand their applications. It has been shown that AIEgens can be constructed based on the TICT mechanism, as TICT formation quenches the emissions of monomers and the restriction of TICT rotations in molecular aggregates recovers bright fluorescence.

To demonstrate the prediction power of our computational approach, we decided to engineer a TICT-based AIEgen, utilizing the BODIPY scaffold. BODIPY dyes exhibit large molar extinction coefficients, and potentially afford high fluorescence brightness in the solids. Moreover, the *meso*-phenyl substituent and the BODIPY scaffold are highly twisted. This steric structure helps to minimize π–π interactions in molecular aggregates and thus avoid aggregation caused quenching (ACQ).

We started with the modeling of Ph-BDP (Figure 6a), which is known to possess bright fluorescence in solutions and solids.[15] Indeed, our calculations show that the highly emissive LE state of Ph-BDP remains the most stable singlet excited state on a flat PES (Figure 6b). The electron and hole distributions of the LE state localize in the BODIPY fragment of Ph-BDP (Figure 6c).

We speculate that the TICT state could be stabilized via introducing an electron-donating group (that is, the azetidine group) to the *meso*-phenyl ring, yielding AZE-Ph-BDP (Figure 6a). With the inclusion of two single bonds in AZE-Ph-BDP, it is challenging to precisely identify the potential rotating bond(s). We have thus scanned the PESs of the LE (S_2) and CT (S_1) states of AZE-Ph-BDP as a function of both θ and φ rotations in tetrahydrofuran (THF, a representative polar solvent; Figure 6b). Our results show that the azetidine ring prefers a planar alignment with respect to the *meso*-phenyl ring ($\varphi = 0°$), and the further rotation of the azetidine group is energetically unfavorable on the S_1 and S_2 PESs. In contrast, the rotation of θ towards 90° is almost barrierless in AZE-Ph-BDP. Consequently, the most stable S_1 conformation is characterized by a perpendicular alignment with a complete charge separation between the azetidine-phenyl group and the BODIPY scaffold, resulting in a negligible oscillator strength ($f = 0.00$; Figure 6c). These features match the typical characteristics of the TICT state.

Experimental Validations of the TICT-based AIEgen

To verify our computational predictions, we synthesized AZE-Ph-BDP and measured its quantum yields in various solvents of different polarities (Supporting Information, Figures S44–47, Scheme S6). Compound AZE-Ph-BDP is emissive only in hexane ($\Phi = 0.36$; Figure 6d). As the solvent polarity increases, the quantum yields of AZE-Ph-BDP become negligible. We next measured the viscosity dependence of the emission intensity in AZE-Ph-BDP, by varying the volume ratio of ethanol and glycerol in the solution (Figure 6e). As expected, the fluorescence of AZE-Ph-BDP greatly intensifies in highly viscous solvents. Both the solvent polarity and viscosity dependence corroborates the TICT formations in AZE-Ph-BDP.

Inspired by the successful prediction of TICT formation, we studied the AIE characteristic of AZE-Ph-BDP in the mixture of dioxane and water with varied volume ratios (Figure 6f). In dioxane, AZE-Ph-BDP is in monomers and the quantum yield is close to 0 (Supporting Information, Figure S48). As the fraction of water increases, the poor solubility of AZE-Ph-BDP in aqueous solution results in the formation of an increasing amount of molecular aggregates. The molecular aggregates effectively inhibit TICT rotations. Consequently, we observed a great enhancement of emission intensities, up to 27 times. Meanwhile, AZE-Ph-BDP also shows bright fluorescence in the solid state ($\Phi = 0.11$; Supporting Information, Figure S49).

Overall, this body of experimental evidence successfully demonstrate the prediction power of our computational approach in developing TICT-based AIEgens.

Conclusion

We have demonstrated a generalizable TD-DFT computational method for the accurate modeling of TICT formations in various fluorophores. The CAM-B3LYP/cLR-SMD level of theory (or other global hybrid functionals with large Hartree–Fock exchange contributions (such as M062X) and range-separated functionals (such as ωB97XD) in combination with the cLR formalism) provides a good description of S_1 PES during the transition from the LE/ICT to TICT states. This computational approach is applicable in a wide range of organic fluorophores (such as naphthalimide, phthalimide, rhodamine, rhodol, acridine, oxazine, NBD, Danysl, coumarin, and BODIPY dyes).

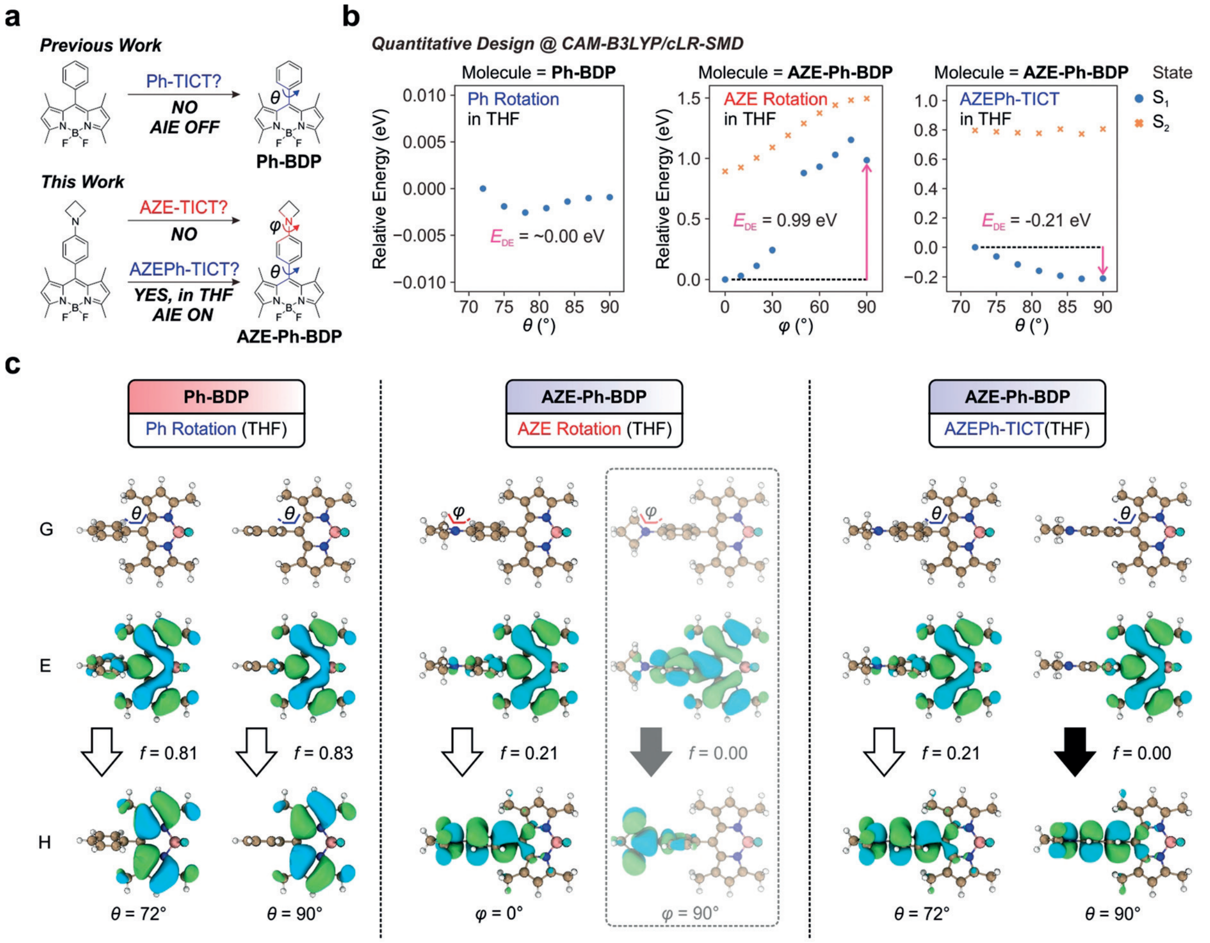

d

Photophysical Properties of **AZE-Ph-BDP**

Solvent	λ_{abs}(nm)	λ_{em}(nm)	$\Delta\lambda$ (nm)	Φ
Hexane	496	509	13	0.36
DCM	500	N. A.	N. A.	~0.00
EtOH	498	N. A.	N. A.	~0.00
ACN	496	N. A.	N. A.	~0.00
DMSO	500	N. A.	N. A.	~0.00

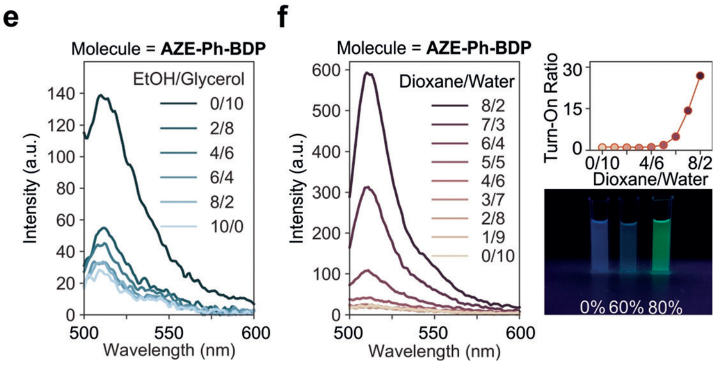

Figure 6. a) A general comparison of the AIE characteristics of BODIPY derivatives reported in previous work (Ph-BDP) and this work (AZE-Ph-BDP). b) Calculated relative energies as functions of Ph or AZEPh (θ) and AZE (φ) rotation angles using the CAM-B3LYP/cLR-SMD level in THF solutions and c) the related molecular geometries (G) and the distributions of electron (E) and hole (H) natural transition orbitals (NTOs). The semi-transparent NTOs indicate that the AZE rotation is not energetically favored in THF. d) UV/Vis absorption (λ_{abs}), emission maxima (λ_{em}), Stokes shifts ($\Delta\lambda$), and quantum yields (Φ) of AZE-Ph-BDP in various solutions. e) The fluorescence intensity of AZE-Ph-BDP as a function of EtOH/glycerol volume fractions. f) The relative fluorescence intensity of AZE-Ph-BDP as a function of dioxane/water volume fractions, the corresponding turn-on ratio for AIE, and photographs of representative samples under UV light in a dark room.

Based on this computational approach, we provided compelling theoretical evidence to show that replacing the dialkylamino group with the azetidinyl moiety weakens the tendency of populating TICT states, thus contributing to improved quantum yields and enhanced photostability of fluorophores. To further validate the reliability of our computational approach, we revisited and concluded a two-decade-long mechanistic debate on PRODAN, by demonstrating that the non-emissive TICT state could form in PRODAN derivatives. This renewed perspective, in combination with TD-DFT predictions, enabled the quantitative computational design of a new P4 derivative with enhanced brightness and photostability by inhibiting TICT. Subsequent experiments validated our computational designs and the TICT mechanism, as well as its excellent one-photon and two-photon bioimaging utilities.

This accurate computational approach further allows us to quantitatively design AIEgens by enabling TICT in monomers and inhibiting such rotations in molecular aggregates. We have successfully demonstrated the prediction power of our computational method, by developing a new AIEgen with a fluorescence turn-on ratio of circa 27 times in aggregates.

We are currently extending the use of our computational approach to other fluorophore systems involving varying degrees of charge transfer. We hope that this work will inspire others in the field of dye chemistry to adopt TD-DFT for the quantitative design of high-performance functional materials.

Acknowledgements

This work is supported by SUTD and the SUTD-MIT International Design Centre (IDC) [T1SRCI17126, IDG31800104], the SUTD-ZJU Research Collaboration Grant (SD201802), the NSFC (21878286, 21908216) and DICP (DMTO201603, TMSR201601). The authors would like to acknowledge the use of the computing service of SUTD-MIT IDC and NSCC.

Conflict of interest

The authors declare no conflict of interest.

Keywords: AIE · azetidinyl substitution · molecular engineering · PRODAN · TICT

[1] a) H. Sunahara, Y. Urano, H. Kojima, T. Nagano, *J. Am. Chem. Soc.* **2007**, *129*, 5597–5604; b) T. Ueno, Y. Urano, K.-i. Setsukinai, H. Takakusa, H. Kojima, K. Kikuchi, K. Ohkubo, S. Fukuzumi, T. Nagano, *J. Am. Chem. Soc.* **2004**, *126*, 14079–14085.

[2] a) D. Jacquemin, E. A. Perpète, I. Ciofini, C. Adamo, *Acc. Chem. Res.* **2009**, *42*, 326–334; b) W. Chi, Q. Qiao, R. Lee, W. Liu, Y. S. Teo, D. Gu, M. J. Lang, Y. T. Chang, Z. Xu, X. Liu, *Angew. Chem. Int. Ed.* **2019**, *58*, 7073–7077; *Angew. Chem.* **2019**, *131*, 7147–7151; c) X. Liu, Z. Xu, J. M. Cole, *J. Phys. Chem. C* **2013**, *117*, 16584–16595.

[3] A. D. Laurent, D. Jacquemin, *Int. J. Quantum Chem.* **2013**, *113*, 2019–2039.

[4] a) A. D. Laurent, C. Adamo, D. Jacquemin, *Phys. Chem. Chem. Phys.* **2014**, *16*, 14334–14356; b) C. Adamo, D. Jacquemin, *Chem. Soc. Rev.* **2013**, *42*, 845–856.

[5] a) R. L. Gieseking, S. Mukhopadhyay, C. Risko, S. R. Marder, J.-L. Brédas, *Adv. Mater.* **2014**, *26*, 68–84; b) Y. Olivier, J. C. Sancho-Garcia, L. Muccioli, G. D'Avino, D. Beljonne, *J. Phys. Chem. Lett.* **2018**, *9*, 6149–6163.

[6] Z.-L. Cai, K. Sendt, J. R. Reimers, *J. Chem. Phys.* **2002**, *117*, 5543–5549.

[7] a) Z. R. Grabowski, K. Rotkiewicz, W. Rettig, *Chem. Rev.* **2003**, *103*, 3899–4032; b) W. Rettig, *Angew. Chem. Int. Ed. Engl.* **1986**, *25*, 971–988; *Angew. Chem.* **1986**, *98*, 969–986.

[8] K. Rotkiewicz, K. H. Grellmann, Z. R. Grabowski, *Chem. Phys. Lett.* **1973**, *19*, 315–318.

[9] a) T. L. Chang, W. L. Borst, *J. Chem. Phys.* **1990**, *93*, 4724–4729; b) K. G. Casey, E. L. Quitevis, *J. Phys. Chem.* **1988**, *92*, 6590–6594; c) T.-L. Chang, H. C. Cheung, *Chem. Phys. Lett.* **1990**, *173*, 343–348; d) A. Barik, M. Kumbhakar, S. Nath, H. Pal, *Chem. Phys.* **2005**, *315*, 277–285; e) G. Jones, W. R. Jackson, C. Y. Choi, W. R. Bergmark, *J. Phys. Chem.* **1985**, *89*, 294–300; f) W. Chi, J. Chen, Q. Qiao, Y. Gao, Z. Xu, X. Liu, *Phys. Chem. Chem. Phys.* **2019**, *21*, 16798–16803; g) X. Liu, Q. Qiao, W. Tian, W. Liu, J. Chen, M. J. Lang, Z. Xu, *J. Am. Chem. Soc.* **2016**, *138*, 6960–6963; h) M. Vogel, W. Rettig, R. Sens, K. H. Drexhage, *Chem. Phys. Lett.* **1988**, *147*, 452–460.

[10] a) J. B. Grimm, B. P. English, J. Chen, J. P. Slaughter, Z. Zhang, A. Revyakin, R. Patel, J. J. Macklin, D. Normanno, R. H. Singer, et al., *Nat. Methods* **2015**, *12*, 244–250; b) S. Singha, D. Kim, B. Roy, S. Sambasivan, H. Moon, A. S. Rao, J. Y. Kim, T. Joo, J. W. Park, Y. M. Rhee, et al., *Chem. Sci.* **2015**, *6*, 4335–4342; c) Z. Ye, W. Yang, C. Wang, Y. Zheng, W. Chi, X. Liu, Z. Huang, X. Li, Y. Xiao, *J. Am. Chem. Soc.* **2019**, *141*, 14491–14495.

[11] S. Sasaki, G. P. C. Drummen, G.-i. Konishi, *J. Mater. Chem. C* **2016**, *4*, 2731–2743.

[12] M. A. Haidekker, T. P. Brady, D. Lichlyter, E. A. Theodorakis, *J. Am. Chem. Soc.* **2006**, *128*, 398–399.

[13] A. Taniguchi, Y. Shimizu, K. Oisaki, Y. Sohma, M. Kanai, *Nat. Chem.* **2016**, *8*, 974.

[14] T. Myochin, K. Hanaoka, S. Iwaki, T. Ueno, T. Komatsu, T. Terai, T. Nagano, Y. Urano, *J. Am. Chem. Soc.* **2015**, *137*, 4759–4765.

[15] R. Hu, E. Lager, A. Aguilar-Aguilar, J. Liu, J. W. Y. Lam, H. H. Y. Sung, I. D. Williams, Y. Zhong, K. S. Wong, E. Peña-Cabrera, et al., *J. Phys. Chem. C* **2009**, *113*, 15845–15853.

[16] G. Bassolino, C. Nançoz, Z. Thiel, E. Bois, E. Vauthey, P. Rivera-Fuentes, *Chem. Sci.* **2018**, *9*, 387–391.

[17] a) C. Jamorski Jödicke, H. P. Lüthi, *J. Am. Chem. Soc.* **2003**, *125*, 252–264; b) D. Rappoport, F. Furche, *J. Am. Chem. Soc.* **2004**, *126*, 1277–1284; c) J. Dreyer, A. Kummrow, *J. Am. Chem. Soc.* **2000**, *122*, 2577–2585; d) B. Mennucci, A. Toniolo, J. Tomasi, *J. Am. Chem. Soc.* **2000**, *122*, 10621–10630.

[18] W. N. Andreas, B. J. Parusel, S. Grimme, G. Köhler, *J. Phys. Chem. A* **1998**, *102*, 7149–7156.

[19] a) B. C. Lobo, C. J. Abelt, *J. Phys. Chem. A* **2003**, *107*, 10938–10943; b) R. K. Everett, H. A. Nguyen, C. J. Abelt, *J. Phys. Chem. A* **2010**, *114*, 4946–4950; c) T. Chen, S. W. Lee, C. J. Abelt, *ACS Omega* **2018**, *3*, 4816–4823.

[20] a) A. Dreuw, J. L. Weisman, M. Head-Gordon, *J. Chem. Phys.* **2003**, *119*, 2943–2946; b) T. Yanai, D. P. Tew, N. C. Handy, *Chem. Phys. Lett.* **2004**, *393*, 51–57; c) J.-D. Chai, M. Head-Gordon, *Phys. Chem. Chem. Phys.* **2008**, *10*, 6615–6620.

[21] R. Li, J. Zheng, D. G. Truhlar, *Phys. Chem. Chem. Phys.* **2010**, *12*, 12697–12701.

[22] R. J. Magyar, S. Tretiak, *J. Chem. Theory Comput.* **2007**, *3*, 976–987.

[23] a) J. Autschbach, M. Srebro, *Acc. Chem. Res.* **2014**, *47*, 2592–2602; b) C. Wang, C. Deng, D. Wang, Q. S. Zhang, *J. Phys. Chem. C* **2018**, *122*, 7816–7823; c) C. Wang, Q. Zhang, *J. Phys. Chem. C* **2019**, *123*, 4407–4416; d) C. Wang, K. Zhou, S. Huang, Q. Zhang, *J. Phys. Chem. C* **2019**, *123*, 13869–13876; e) T. J. Penfold, *J. Phys. Chem. C* **2015**, *119*, 13535–13544.

[24] a) C. A. Guido, B. Mennucci, D. Jacquemin, C. Adamo, *Phys. Chem. Chem. Phys.* **2010**, *12*, 8016–8023; b) G.-J. Zhao, K.-L. Han, *Phys. Chem. Chem. Phys.* **2010**, *12*, 8914–8918.

[25] P. Wiggins, J. A. G. Williams, D. J. Tozer, *J. Chem. Phys.* **2009**, *131*, 091101.

[26] W. Rettig, M. Zander, *Chem. Phys. Lett.* **1982**, *87*, 229–234.

[27] C. A. Guido, D. Jacquemin, C. Adamo, B. Mennucci, *J. Chem. Theory Comput.* **2015**, *11*, 5782–5790.

[28] a) D. Kats, T. Korona, M. Schütz, *J. Chem. Phys.* **2006**, *125*, 104106; b) D. Kats, M. Schütz, *J. Chem. Phys.* **2009**, *131*, 124117.

[29] S. Nad, M. Kumbhakar, H. Pal, *J. Phys. Chem. A* **2003**, *107*, 4808–4816.

[30] P. Hazra, D. Chakrabarty, N. Sarkar, *Langmuir* **2002**, *18*, 7872–7879.

[31] E. Lippert, W. Rettig, V. Bonačić-Koutecký, F. Heisel, J. Miehé, *Adv. Chem. Phys.* **1987**, *68*, 1 – 174.

[32] T. von Der Haar, A. Hebecker, Y. Il'Ichev, Y.-B. Jiang, W. Kühnle, K. A. Zachariasse, *Recl. Trav. Chim. Pays-Bas* **1995**, *114*, 430 – 442.

[33] G. Weber, F. J. Farris, *Biochemistry* **1979**, *18*, 3075 – 3078.

[34] a) T. Parasassi, E. K. Krasnowska, L. Bagatolli, E. Gratton, *J. Fluoresc.* **1998**, *8*, 365 – 373; b) E. Benedetti, L. S. Kocsis, K. M. Brummond, *J. Am. Chem. Soc.* **2012**, *134*, 12418 – 12421; c) O. A. Kucherak, P. Didier, Y. Mély, A. S. Klymchenko, *J. Phys. Chem. Lett.* **2010**, *1*, 616 – 620.

[35] a) A. B. J. Parusel, W. Nowak, S. Grimme, G. Köhler, *J. Phys. Chem. A* **1998**, *102*, 7149 – 7156; b) M. Viard, J. Gallay, M. Vincent, O. Meyer, B. Robert, M. Paternostre, *Biophys. J.* **1997**, *73*, 2221 – 2234; c) M. Novaira, M. A. Biasutti, J. J. Silber, N. M. Correa, *J. Phys. Chem. B* **2007**, *111*, 748 – 759; d) M. Pederzoli, L. Sobek, J. Brabec, K. Kowalski, L. Cwiklik, J. Pittner, *Chem. Phys. Lett.* **2014**, *597*, 57 – 62.

[36] B. Mennucci, M. Caricato, F. Ingrosso, C. Cappelli, R. Cammi, J. Tomasi, G. Scalmani, M. J. Frisch, *J. Phys. Chem. B* **2008**, *112*, 414 – 423.

[37] C. J. Abelt, T. Sun, R. K. Everett, *Photochem. Photobiol. Sci.* **2011**, *10*, 618 – 622.

[38] a) Y. Yang, D. Li, C. Li, Y. Liu, K. Jiang, *Spectrochim. Acta Part A* **2017**, *187*, 68 – 74; b) I. G. Alty, D. W. Cheek, T. Chen, D. B. Smith, E. Q. Walhout, C. J. Abelt, *J. Phys. Chem. A* **2016**, *120*, 3518 – 3523.

[39] S. Saha, A. Samanta, *J. Phys. Chem. A* **1998**, *102*, 7903 – 7912.

[40] Y. Marcus, *Chem. Soc. Rev.* **1993**, *22*, 409 – 416.

[41] a) Y. Dong, J. W. Y. Lam, A. Qin, J. Liu, Z. Li, B. Z. Tang, J. Sun, H. S. Kwok, *Appl. Phys. Lett.* **2007**, *91*, 011111; b) W. Qin, Z. Yang, Y. Jiang, J. W. Y. Lam, G. Liang, H. S. Kwok, B. Z. Tang, *Chem. Mater.* **2015**, *27*, 3892 – 3901; c) J. Guo, X.-L. Li, H. Nie, W. Luo, R. Hu, A. Qin, Z. Zhao, S.-J. Su, B. Z. Tang, *Chem. Mater.* **2017**, *29*, 3623 – 3631; d) Z. Ning, Z. Chen, Q. Zhang, Y. Yan, S. Qian, Y. Cao, H. Tian, *Adv. Funct. Mater.* **2007**, *17*, 3799 – 3807; e) B. Liu, H. Nie, X. Zhou, S. Hu, D. Luo, D. Gao, J. Zou, M. Xu, L. Wang, Z. Zhao, et al., *Adv. Funct. Mater.* **2016**, *26*, 776 – 783.

[42] a) B. Gu, W. Wu, G. Xu, G. Feng, F. Yin, P. H. J. Chong, J. Qu, K.-T. Yong, B. Liu, *Adv. Mater.* **2017**, *29*, 1701076; b) Y. Yuan, C.-J. Zhang, M. Gao, R. Zhang, B. Z. Tang, B. Liu, *Angew. Chem. Int. Ed.* **2015**, *54*, 1780 – 1786; *Angew. Chem.* **2015**, *127*, 1800 – 1806; c) M. Li, Y. Gao, Y. Yuan, Y. Wu, Z. Song, B. Z. Tang, B. Liu, Q. C. Zheng, *ACS Nano* **2017**, *11*, 3922 – 3932; d) C.-J. Zhang, Q. Hu, G. Feng, R. Zhang, Y. Yuan, X. Lu, B. Liu, *Chem. Sci.* **2015**, *6*, 4580 – 4586; e) C.-C. Chang, M.-C. Hsieh, J.-C. Lin, T.-C. Chang, *Biomaterials* **2012**, *33*, 897 – 906.

[43] a) R. T. K. Kwok, C. W. T. Leung, J. W. Y. Lam, B. Z. Tang, *Chem. Soc. Rev.* **2015**, *44*, 4228 – 4238; b) K. Han, S.-B. Wang, Q. Lei, J.-Y. Zhu, X.-Z. Zhang, *ACS Nano* **2015**, *9*, 10268 – 10277; c) M. Wang, G. Zhang, D. Zhang, D. Zhu, B. Z. Tang, *J. Mater. Chem.* **2010**, *20*, 1858 – 1867; d) X. Wang, J. Hu, G. Zhang, S. Liu, *J. Am. Chem. Soc.* **2014**, *136*, 9890 – 9893; e) X. Jia, X. Yang, J. Li, D. Li, E. Wang, *Chem. Commun.* **2014**, *50*, 237 – 239.

Manuscript received: December 19, 2019
Accepted manuscript online: January 13, 2020
Version of record online: February 3, 2020